

THERMAL TRANSPORT IN SELF-ASSEMBLED NANOSTRUCTURES

BY

IAN PEARSON BLITZ

THESIS

Submitted in partial fulfillment of the requirements
for the degree of Master of Science in Chemistry
in the Graduate College of the
University of Illinois at Urbana-Champaign, 2011

Adviser:

Professor Paul V. Braun

Report Documentation Page

Form Approved
OMB No. 0704-0188

Public reporting burden for the collection of information is estimated to average 1 hour per response, including the time for reviewing instructions, searching existing data sources, gathering and maintaining the data needed, and completing and reviewing the collection of information. Send comments regarding this burden estimate or any other aspect of this collection of information, including suggestions for reducing this burden, to Washington Headquarters Services, Directorate for Information Operations and Reports, 1215 Jefferson Davis Highway, Suite 1204, Arlington VA 22202-4302. Respondents should be aware that notwithstanding any other provision of law, no person shall be subject to a penalty for failing to comply with a collection of information if it does not display a currently valid OMB control number.

1. REPORT DATE 2011	2. REPORT TYPE	3. DATES COVERED 00-00-2011 to 00-00-2011		
4. TITLE AND SUBTITLE Thermal Transport in Self-Assembled Nanostructures			5a. CONTRACT NUMBER	
			5b. GRANT NUMBER	
			5c. PROGRAM ELEMENT NUMBER	
6. AUTHOR(S)			5d. PROJECT NUMBER	
			5e. TASK NUMBER	
			5f. WORK UNIT NUMBER	
7. PERFORMING ORGANIZATION NAME(S) AND ADDRESS(ES) University of Illinois at Urbana-Champaign, Urbana, IL, 61801			8. PERFORMING ORGANIZATION REPORT NUMBER	
9. SPONSORING/MONITORING AGENCY NAME(S) AND ADDRESS(ES)			10. SPONSOR/MONITOR'S ACRONYM(S)	
			11. SPONSOR/MONITOR'S REPORT NUMBER(S)	
12. DISTRIBUTION/AVAILABILITY STATEMENT Approved for public release; distribution unlimited				
13. SUPPLEMENTARY NOTES				
14. ABSTRACT Understanding of phonon mediated thermal transport properties in nanostructured materials is essential for the intelligent design of next-generation microelectronic and thermoelectric devices. Presented here is the study of the thermal transport properties of model organic/inorganic nanoscopically layered systems for the purpose of elucidating the dependence of bulk thermal conductivity on the nanostructure of the material and, specifically, the role that limited interfacial thermal conductance plays. We measured the bulk thermal conductivity of various organically modified montmorillonite clays as a function of several variables. Thermal conductivities of the organically modified clays were measured to be approximately 0.09 W/mK and were relatively independent of the variables investigated. This suggests the dominance of the organic-inorganic interfacial conductance in the determination of bulk thermal conductivity of this system and was determined from the thermal conductivity measurements to be approximately 150 MW/m²K, which is consistent with measured interfacial conductance in similarly coupled systems. Organic-inorganic perovskite structures were also investigated to determine the effect that varying crystal structure plays in determining thermal bulk thermal conductivity. While the data is too sparse to draw strong conclusions, current data suggests little dependence on the subtle changes in the crystal structure observed here. However, further study of this system may be warranted.				
15. SUBJECT TERMS				
16. SECURITY CLASSIFICATION OF:			17. LIMITATION OF ABSTRACT Same as Report (SAR)	
a. REPORT unclassified	b. ABSTRACT unclassified	c. THIS PAGE unclassified		
18. NUMBER OF PAGES 45	19a. NAME OF RESPONSIBLE PERSON			

ABSTRACT

Understanding of phonon mediated thermal transport properties in nanostructured materials is essential for the intelligent design of next-generation microelectronic and thermoelectric devices. Presented here is the study of the thermal transport properties of model organic-inorganic, nanoscopically layered systems for the purpose of elucidating the dependence of bulk thermal conductivity on the nanostructure of the material and, specifically, the role that limited interfacial thermal conductance plays. We measured the bulk thermal conductivity of various organically modified montmorillonite clays as a function of several variables. Thermal conductivities of the organically modified clays were measured to be approximately 0.09 W/mK and were relatively independent of the variables investigated. This suggests the dominance of the organic-inorganic interfacial conductance in the determination of bulk thermal conductivity of this system and was determined from the thermal conductivity measurements to be approximately 150 MW/m²K, which is consistent with measured interfacial conductance in similarly coupled systems.

Organic-inorganic perovskite structures were also investigated to determine the effect that varying crystal structure plays in determining thermal bulk thermal conductivity. While the data is too sparse to draw strong conclusions, current data suggests little dependence on the subtle changes in the crystal structure observed here. However, further study of this system may be warranted.

ACKNOWLEDGEMENTS

First and foremost, I would like to thank Prof. Paul Braun for all his help and understanding throughout my time in his group. I would also like to thank the all members, past and present, of the Braun group, and Dr. Mark Losego and Dr. Dara Gough in particular, for all their help and company. Additionally, the Cahill group was instrumental in helping me to learn virtually all the material that I have learned here and I owe them my gratitude.

This work was funded by U.S. Air Force Office of Scientific Research MURI Grant FA9550-08-1-0407.

TABLE OF CONTENTS

CHAPTER 1: INTRODUCTION	1
1.1 Thermal Conductivity and Thermal Boundary Conductance	1
1.2 Nanoscale Layered Materials.....	3
1.3 Time-domain Thermoreflectance.....	5
1.4 Figures.....	7
CHAPTER 2: THERMAL TRANSPORT IN ORGANICALLY MODIFIED MONTMORILLONITES	10
2.1 Background.....	10
2.2 Preparation and Characterization.....	11
2.1.1 Synthesis of Organically Modified Clays	11
2.1.2 Organoclay Film Preparation and Characterization.....	12
2.3 Calculation of Thermal Conductivities and Error.....	14
2.4 Thermal Conductivity Measurements of Organically Modified Clay Films	16
2.5 Temperature Dependent Thermal Conductivity Measurements	17
2.6 Discussion	18
2.7 Figures.....	21
CHAPTER 3: THERMAL TRANSPORT IN SnI_6 – ORGANIC LAYERED PEROVSKITES	34
3.1 Background.....	34
3.2 Synthesis and Characterization of SnI_6 Perovskites.....	34
3.3 Thermal Conductivity Measurements of SnI_6 – Organic Perovskite Films	35
3.4 Discussion	36
3.5 Figures.....	37
CHAPTER 4: CONCLUSIONS	39
LIST OF REFERENCES	41

CHAPTER 1

INTRODUCTION

1.1 Thermal Conductivity and Thermal Boundary Conductance

Heat management is a concern in nearly every branch of practical engineering, from microelectronics to architecture. Dissipation or concentration of thermal energy is a requirement for the efficient design of devices for a wide variety of applications. To best facilitate efficient management of thermal energy, the design of materials with desirable thermal transport properties is essential.

The most useful description of a material's thermal transport properties is its thermal conductivity, Λ . The thermal conductivity is traditionally defined by Fourier's Law of heat conduction which states that the rate of heat energy transfer through a material is proportional to the negative gradient in the temperature field where the thermal conductivity is the proportionality constant. In the case of most bulk materials, this thermal conductivity is a function of the material's atomic composition and crystal structure, where more uniformly crystalline materials display higher thermal conductivities than less ordered, glassy materials. However, Fourier's Law is a stochastic description and becomes invalid at areas of high anisotropy, such as interfacial boundaries, and as nanoscopic length scales are approached. Through the manipulation of material properties and boundaries at the nanoscale, the thermal transport behavior of materials can be controlled to a greater extent than ever before. Perhaps the simplest way to modify the thermal transport behavior of materials in this fashion is through the control of interfacial boundaries and boundary density.

Interfacial boundary resistance has been a subject of study since it was first proposed to be significant by Keesom and Keesom in 1936 and experimentally measured by Kaptiza at a liquid

helium – bronze interface in 1941.^{1,2} Since that time, the study of thermal transport at interfaces has become quite important with the advent of solid-state electronics of ever decreasing dimension.

A thermal boundary resistance, typically measured in thermal power through an area per a temperature difference, (often reported in the units $\text{MW}/\text{m}^2\text{K}$) is characterized by a discontinuity in the temperature field at an interface that is subjected to a temperature gradient (Figure 1a) and has been traditionally difficult to predict.³ The two oldest and most conventional models of interfacial conductance are the acoustic mismatch model and the diffuse mismatch model which generally form the bounds for the expected experimental value. The acoustic mismatch model determines interfacial conductance by the ratio of acoustic impedance between the two materials forming the interface, much in the same way that optical reflectance is classically determined by the difference in index of refraction at an interface.⁴ The acoustic mismatch model usually represents the lower limit on expected interfacial conductance. The diffuse mismatch model determines interfacial conductance by the ratio between the phonon density of states for any given phonon frequency and usually represents the upper limit of predicted interfacial conductance.⁵ As evidenced by this lack of ability to accurately predict interfacial thermal transport behavior, interfacial effects are not well understood.

While it may not yet be possible to accurately predict the interfacial thermal boundary conductance between arbitrary materials, through the use of modern analytic techniques, such as time-domain thermoreflectance, which will be discussed in more detail in a later section, boundary conductance across very strongly mismatched boundaries have been measured to have exceptionally low conductances such as the Pb/hydrogen terminated diamond interface which has the lowest measured interfacial conductance of less than $20 \text{ MW}/\text{m}^2\text{K}$.⁶ Coupled with high

interface densities, even relatively high interfacial conductances will produce measurably reduced bulk thermal conductivities; a technique that has already been applied to the development of high figure-of-merit thermoelectric devices through high interface density semiconductor superlattices.⁷

1.2 Nanoscale Layered Materials

Until recently, the lower limit to a material's thermal conductivity was believed to be set by the so-called "amorphous limit" which describes the thermal conductivity of an amorphous material as a random walk of vibrational energy between neighboring atoms.⁸ Recent work has demonstrated that through nanoscale material design the thermal conductivity can be pushed below the amorphous limit.^{9, 10}

An important class of ultralow thermal conductivity materials are those formed from nanoscale superlattices having alternating layers with differing acoustic properties. A significant amount of work has gone into studying thermal transport in semiconductor superlattices due to their applications to the development of high figure-of-merit thermoelectric materials. Numerous groups have studied the effects of varying layer thickness in systems with repeat spacings longer than the phonon mean-free-path. In these cases, the thermal conductivity of the overall superlattice is reduced by the limited conductance at each interface.^{11, 12} However the thermal transport properties of superlattices with layer thicknesses that approach the phonon mean-free-path are poorly understood. Theoretically, coherent phonon reflection off multiple interfaces could result in phonon minibands, which would increase the transmission coefficient of phonons of the appropriate wavelength across the boundaries but with a reduced group

velocity, thereby increasing the thermal conductivity.^{13, 14} Though some groups have observed this to be the case^{15, 16}, others have shown that the thermal conductivity of such short period superlattices continues to decrease as the layer thickness is decreased.^{17, 18} The high interface-density limit of this class of materials has been studied by Chiritescu *et al.* for ordered WSe₂ films in which each layer is 3 atoms (< 1 nm) thick. This system showed the lowest measured thermal conductivity of any fully dense solid with a lowest thermal conductivity of 0.05 W/mK (Figure 2b).¹⁰

However, measuring the thermal conductivity as a function of layer thickness at these dimensions is quite difficult. The WSe₂ superlattice system and other related ultra-low thermal conductivity superlattice systems were synthesized using molecular beam epitaxy (MBE) or metal-organic chemical vapor deposition (MOCVD) which, while providing excellent control over layer thickness and uniformity, limit material choices to inorganics and limit the possible types of interfacial interactions.^{10, 11} This work describes the synthesis and measurement of the effective thermal conductivity of a self-assembled, organic-inorganic nanoscopic superlattice for the purpose of studying the effect that the interfacial boundary conductance and boundary density has on phonon mediated heat transport.

The measurement of the thermal conductivity of these composite materials is made possible through the use of the time-domain thermoreflectance technique described in the subsequent section.

1.3 Time-domain Thermoreflectance

Time-domain thermoreflectance (TDTR) is a pump-probe laser technique used primarily for the determination of thermal conductivity of solid samples.^{6,19} In a TDTR measurement, the pump pulse heats the sample (or a thin metal film on the surface of the film that acts as a transducer) and the time-delayed probe pulse measures the change in the reflectivity of the surface that arises from the temperature dependence of the optical constants. On the basis of the temperature decay over time being measured at the surface, thermal conductivity of the sample can be determined as long as the dimensions and volumetric heat capacity of the sample is known through comparison to a thermal diffusion model.⁶ The overall optical setup is represented in Figure 3.

In our implementation of TDTR a mode-locked Ti:sapphire laser produces a train of pulses < 500 fs in duration with a repetition rate of 80.6 MHz. This pulse train is split into pump and probe lines on the basis of orthogonal polarization. The optical path length of the pump line is adjusted by way of a mechanical delay stage, the intensity of which is modulated by an electro-optic modulator. The probe line is modulated by a mechanical chopper. The pump and probe lines are then recombined by a polarizing beam-splitter so that a single objective lens can be used to focus both lines onto the sample and to collect the reflection of the probe pulses.²⁰ For all TDTR measurements, the Ti:sapphire output has a wavelength of 787 nm. For the nanostructured film samples, we use pump and probe beam powers of 14 mW and 7 mW respectively and a $1/e^2$ beam radius of 8 μm or 15 μm . The differences in reflected probe pulse intensity due to heating caused by the pump pulse are extracted by a radio frequency lock-in amplifier set to the modulation frequency of the pump beam (9.8 MHz).²⁰ The output of the lock-in amplifier is then measured with audio frequency lock-in amplifiers that are locked to the

frequency of the mechanical chopper. This technique of double modulation greatly increases signal-to-noise ratio and reduces artifacts caused by pump light scattered by the surface of the samples.²¹

1.4 Figures

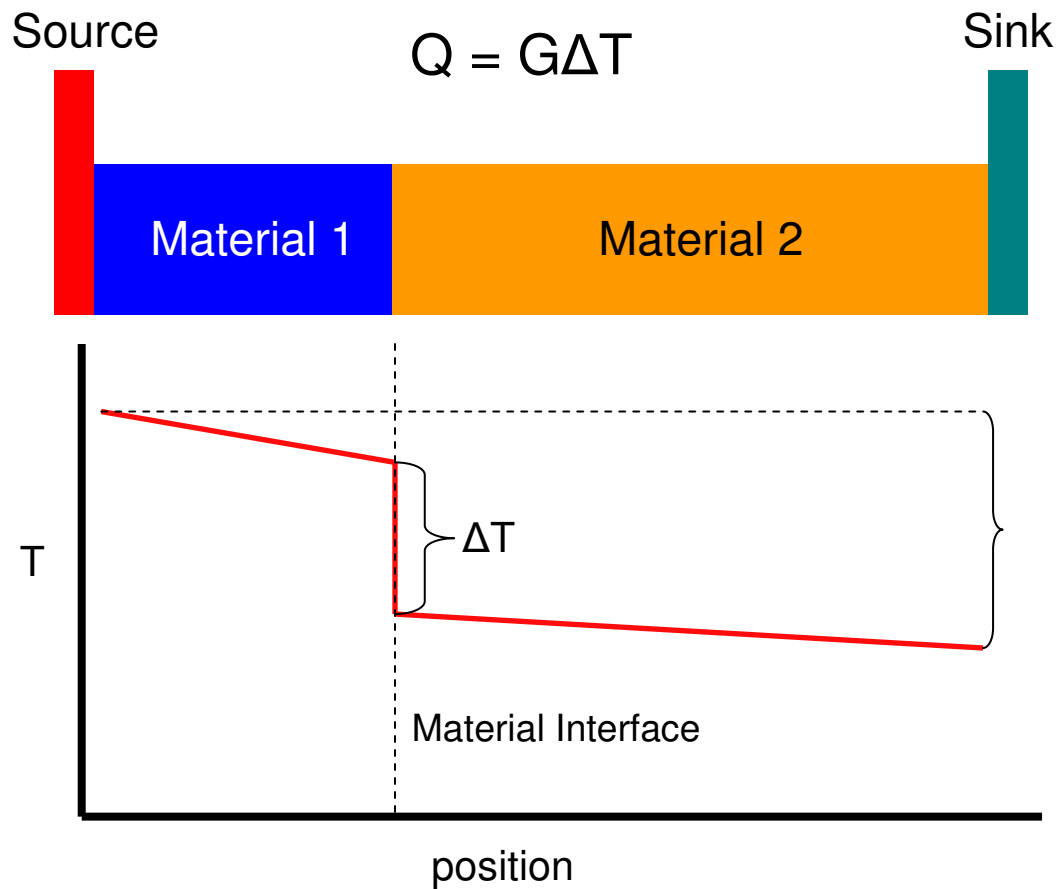
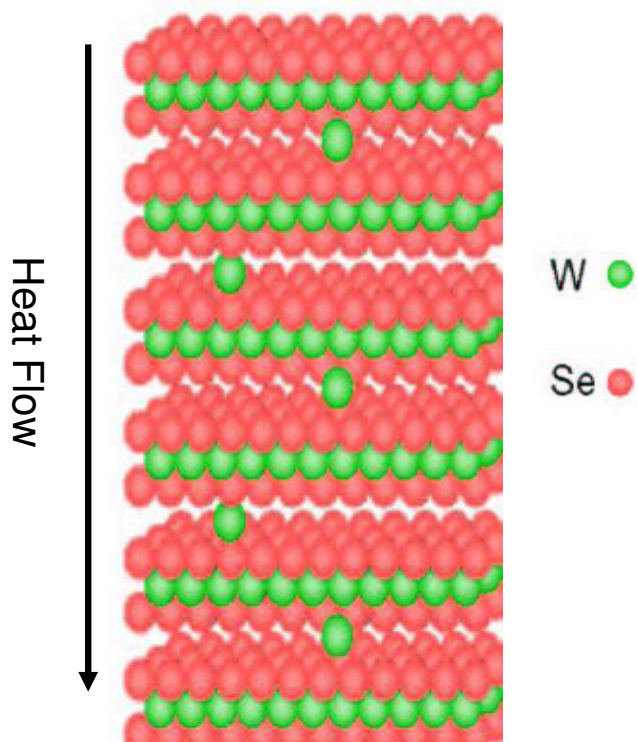


Figure 1: Schematic representing the temperature profile across an interface between two dissimilar materials illustrating the effect that limited boundary conductance has on the temperature profile.

a



b

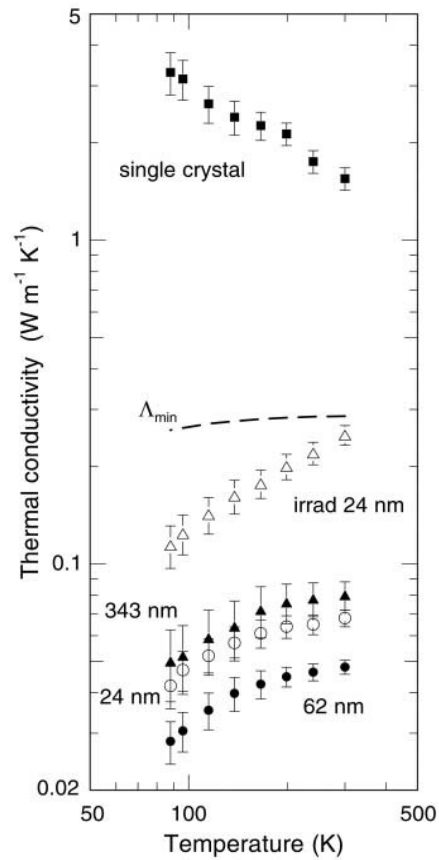


Figure 2: a. Schematic representing the structure of the WSe_2 crystals studied by Chiriteșcu *et al.* and the direction in which the thermal transport properties were measured. b. Thermal conductivity data from Chiriteșcu *et al.* on WSe_2 thin films, showing ultra-low thermal conductivity, below the predicted minimum of the amorphous limit.

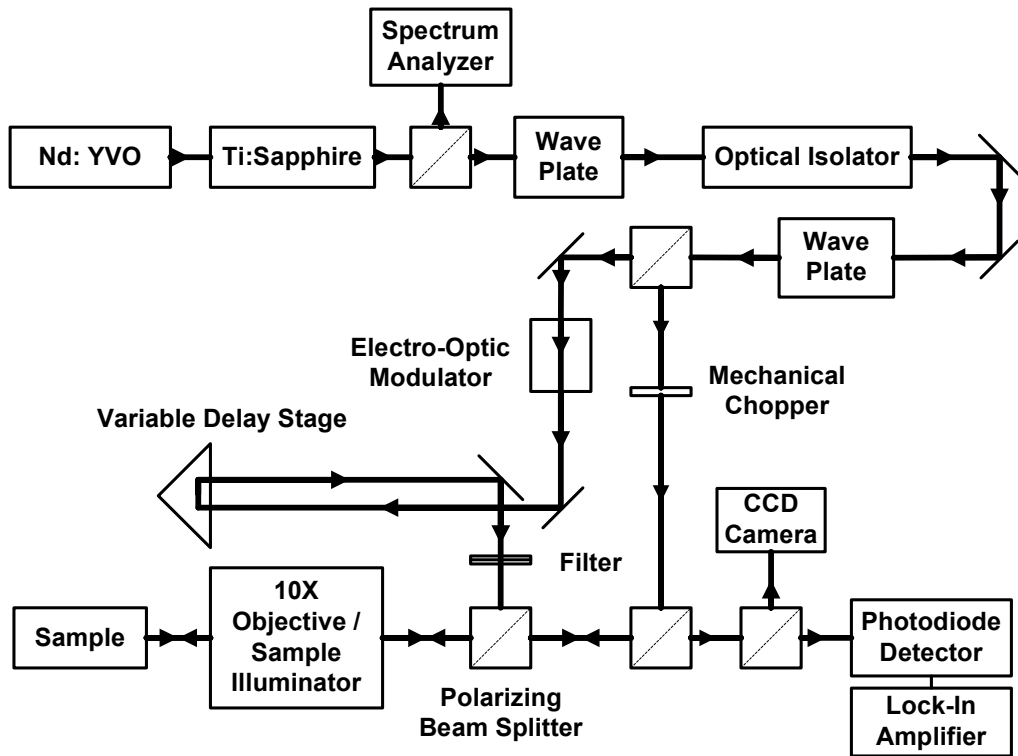


Figure 3: Diagram of the basic time-domain thermoreflectance setup that was used for thermal conductivity measurements.

CHAPTER 2

THERMAL TRANSPORT IN ORGANICALLY MODIFIED MONTMORILLONITES

2.1 Background

Organically modified montmorillonite presents a unique material for studying thermal conductivity in a nanoscale superlattice system. Montmorillonite is a natural layered clay that belongs to the 2:1 smectite clay family which can be exfoliated into large aspect ratio (>1000:1) ~1 nm thick sheets (Figure 4a). Each montmorillonite sheet consists of an octahedral alumina layer sandwiched by two tetrahedral silica layers. Additionally each aluminosilicate particle possesses negative charges, due to Mg^{2+} impurities in the central alumina layer, which are balanced by electrostatically bound Na^+ . The necessity of charge balancing cations provides the opportunity for chemical modification via cation exchange under the appropriate conditions (Figure 4b).²²

The chemical modification of clays via ion exchange is not a novel concept and has been studied extensively, most frequently with the object of creating nanocomposite materials.²² One of the most thoroughly investigated aspects of intercalated clay systems is the effect that various intercalants have on the clay's (001) d-spacing due to the insight this information can give into the packing structure of the interlayer molecules.²³ Investigation into this aspect of chemically modified clay systems has shown that upon intercalation with long-chain primary alkylammonium salts, the (001) d-spacing increases accordingly (Figure something).²³ Due to the nanoscopic dimensions of the clay sheets and of the according interlayers in appropriately chemically modified montmorillonite, an organically modified clay system provides an ideal

structure in which to study the effects of layer thickness and the organic interfacial conductance on the bulk thermal transport properties.

It should be noted that although the work presented here on organically modified clays is restricted to modified montmorillonites, there are numerous other clays that would be suitable for similar study. We chose montmorillonite specifically because of the extensive work previously done on the organically modified systems as well as the ready availability and high purity of montmorillonite. As the only physical requirement for a clay to be chemically modifiable through this process is a high cation exchange capacity (>90 milliequivalents/100 g), similar studies with other mineral components, such as vermiculite or synthetic clays, may be reasonable to pursue in the future.

2.2 Preparation and Characterization

2.2.1 Synthesis of Organically Modified Clays

Organically modified clays were synthesized via an ion exchange reaction between the charge balancing sodium ions and long chain alkylammonium salts of varying length, from decyl- to octadecyl-, and termination. The exchange took place in 5:1 excess alkylammonium salt in 1:1 water/ethanol by volume at 75 °C for 12 hours.²⁴ θ - 2θ x-ray diffraction measurements of the modified clays showed that upon intercalation with organic groups, the clays show an increase in (001) d – spacing in related to the length of the intercalated organic group (Figure 5).

2.2.2 Organoclay Film Preparation and Characterization

In order to study the effects of boundaries on the bulk thermal properties of organo-clay nanostructures, thin films of organically modified clay were prepared. 2% weight dispersions of organically modified clay in a 10:1 mixture of toluene and methanol were spin-coated onto silicon substrates. Films prepared in this manner were between 100 and 400 nm thick depending on spin-coating conditions. Spin coated films were dried under vacuum at 150 °C for 24 hours to remove toluene and methanol from the film. After drying, approximately 65 nm of aluminum metal was sputter deposited onto the clay surface for the TDTR measurements, resulting in the sample geometry represented in Figure 6a.

TDTR measurements on these films proved to be misleading and inconclusive for several reasons. Firstly, films prepared in this manner showed a long period oscillation in the TDTR signal that begins at approximately 300 ps as is evident in Figure 6b. Previous unpublished work by Cahill *et al.* showed that similar, less intense oscillations arise in TDTR measurements of rough films, though they were unable to identify the source of the signal. Considering that we believe this signal to be created by surface roughness it is reasonable to assume that the clay particles at the surface are not well aligned with substrate. Due to the highly anisotropic thermal conductivity of clay multilayers, clay particles misaligned with respect to the substrate would provide an efficient pathway for heat conduction away from the surface, resulting in a higher than minimum measured thermal conductivity. Additionally, the measured thermal conductivities as a function of (001) spacing showed an anomalous decrease as spacing increased, diverging from values predicted by a simple series thermal resistor model using accepted thermal conductivity values for montmorillonite and liquid dodecane, which will be discussed in detail in a later section. It was determined that clay films would have to be extremely smooth and have

well aligned clay particles within the top approximately 25 nm of the film to provide meaningful TDTR data.

To create samples with surfaces sufficiently smooth for accurate TDTR measurement, we developed a multistep sample preparation technique similar to micro-transfer printing. After deposition and drying of the clay film, 10 nm of chromium metal followed by 300 nm of gold were sputtered onto the clay film. ~3 μm of nickel was then electrodeposited onto the gold surface and subsequently attached to a glass slide with a thermally conductive adhesive. Due to the low adhesion between the clay film and the silicon substrate, the silicon substrate can be removed, exposing the surface that was in contact with the silicon surface. This new surface (the geometry of which is represented in Figure 7a) proved to be both smooth enough for TDTR measurement (as evidenced by both SEM images and the elimination of the anomalous TDTR signal as evidenced in Figures 7b and Figure 8) and very well aligned (as evidenced by cross-sectional TEM shown in Figure 9).

Additional information concerning the alignment of the clay in the films is provided by ω – rocking curve x-ray diffraction measurements about the (001) reflection. The rocking curve measurements show what we believe to be two superimposed distributions: a sharp (FWHM $\sim 0.25^\circ$) distribution is observed at $\theta = \omega$ which we believe corresponds to the highly aligned clay particles near the Si surface, and a wider (FWHM $> 1^\circ$) centered at $\theta = \omega$ likely corresponding to more disordered clay sheets deeper into the film (Figure 10). However, we believe the wider distribution is irrelevant to the thermal conductivity measurement because the thermal probe depth does not sample these regions of the film.

Furthermore, DSC measurements of the organically modified clays show a weak glass-transition at approximately 85 degrees Celsius, supporting the conclusion that the organic component of the structure is glassy at room temperature (Figure 11).

The density of the organically modified clay films was confirmed to be consistent with a weighted average between the bulk density values of the organic component and the clay calculated from areal density obtained He^{2+} RBS measurements and profilometry measurements of the film thickness. A typical RBS measurement and the according simulation used for density calculations is represented in Figure 12. This supports the conclusion that the clay films are dense and measurements of low thermal are not due to voids within the film artificially increasing the phonon path length. This conclusion is also supported by cross-sectional TEM measurements that confirm that voids are not present within the probe depth of the TDTR measurements (Figure 9).

2.3 Calculation of Thermal Conductivities and Error

In order to obtain values for the thermal conductivity from raw TDTR data, the data is compared to the output of a diffusive thermal model (Figure 13a). This model is dependent on several variables including layer thickness, thermal conductivity, density, and heat capacity of each element of the model. In the model that we used there are three layers, the “absorption layer”, the aluminum layer corresponding to the aluminum deposited onto the sample, and an infinitely thick sample layer. The absorption layer does not correspond to anything physical and is just a construct in the simulation to decrease the difficulty of the calculation. The absorption layer is set to be 1 nm thick and have thermal conductivity and volumetric heat capacity ten times greater than that of the aluminum layer. Because the absorption layer is actually part of the

aluminum layer, the thickness of the aluminum layer is decreased accordingly, by 10 nm. Since every variable in this model is known, either through measurement or reasonable estimation, save for the thermal conductivity of the sample, the thermal conductivity can be determined by fitting the curve of the model to the data.

While the thermal conductivities, thicknesses, and volumetric heat capacities are known to a reasonable degree for each component of the system (save the thermal conductivity of the sample), obtaining these values is non trivial in some cases. Two of the most critical values in the model other than the parameter being solved for are the thermal conductivity and thickness of the transducer/thermometer aluminum film on the surface of the sample. The thermal conductivity of the aluminum film is calculated from the electrical conductivity of a similar film deposited onto a glass slide at the same time the film was deposited onto the sample using the Wiedemann-Franz law which relates the two quantities. The electrical conductivity is measured using the four-point probe method. The thickness of the aluminum film is measured during the TDTR experiment itself. During the first \sim 100 ps, periodic peaks are visible in the data that correspond to acoustic reflections of the stress-strain wave generated by the laser pulse off of the aluminum clay boundary, which are clearly visible in Figures 7 and 14. Using the speed of sound in aluminum (\sim 6.42 nm/ps) and the time elapsed between reflections, we are able to calculate the local thickness of the film with a high degree of accuracy. The aluminum films are deposited to be approximately 65 nm thick so as to be thick enough to prevent any optical bleed-through to the sample while simultaneously optimizing the sensitivity of the measurement to the thermal conductivity of the sample.

Figure 13b shows the dependence of the sensitivity of the model as a function of the clay layer thickness. The sensitivity of the model to a variable is defined as the partial derivative of

the natural logarithm of the TDTR output ratio with respect to the natural logarithm of the desired variable. This plot shows that the sensitivity of the model to the clay-Al interface and the clay thickness become negligible as the clay film thickness is increased past 50 nm. It is for this reason that all thermal conductivity measurements were made on films >100 nm thick.

It can also be shown that the model is largely only sensitive to the top 25 nm of the clay film, assuming that the clay film has a thermal conductivity of 0.1 W/mK or less. This supports the conclusion that having a highly aligned clay film near the surface with more misalignment deeper into the film is sufficient for accurate measurement of the thermal conductivity normal to the film alignment.

The error in the measurement of the thermal conductivity is calculated through the sensitivities of the model to the various variables. To calculate the error in the thermal conductivity measurement that arises from any variable, the ratio of the sensitivity to the variable to the sensitivity to the thermal conductivity of the sample. This ratio is then multiplied by the calculated value of thermal conductivity, providing the error in the measurement due to the variable in question. The overall error is calculated by summing the errors accumulated from the individual variables, on average resulting in 15 – 20% error.

2.4 Thermal Conductivity Measurements of Organically Modified Clay Films

To investigate the relationship between the thermal conductivity and organic layer thickness, the length of the alkylammonium molecule was varied from 10 to 18 carbon atoms in length. The spacing between aluminosilicate sheets increased from 0.17 to 0.68 nm with increasing alkyl chain length, as verified by θ -2 θ x-ray diffraction measurements (Fig 5b). Thermal measurements of the organic-clay films show the thermal conductivities to all be approximately

0.09 W/mK (Fig 15), approximately 50% lower than the thermal conductivity of the organic layer (dodecane (l) = 0.13 W/mK)²⁵ and 5 times lower than the thermal conductivity of the unmodified clay (0.48 W/mK)²⁶ it should be noted that the thermal conductivity of the montmorillonite is highly anisotropic and the measured value is the thermal conductivity normal to a stack of clay platelets. The thermal conductivity within each montmorillonite sheet is certainly much greater, and may even be comparable to the thermal conductivity of bulk sapphire (>20 W/mK).²⁶

In addition to measuring the thermal conductivity of the organically-modified clay multilayers as a function of intercalant chain length and therefore (001) d-spacing, we measured the thermal conductivity of a series of modified clays with comparable d-spacing but with varying trialkyl functionalizations in addition to a dodecyl- chain (Figure 16).

2.5 Temperature Dependent Thermal Conductivity Measurements

Thermal conductivity of the primary amine modified clays was measured as a function of temperature between room temperature and 110 C to probe the effect that the change in organic chain mobility associated with the glass transition measured via DSC has on the bulk thermal conductivity of the films. As it is impossible to take full TDTR scans at a high enough frequency to represent a reasonable temperature change rate due to the speed of the mechanical delay stage, a modified procedure was used for these experiments. The TDTR setup was set to continuously collect data at 1Hz while the mechanical delay stage was set to stay at a probe pulse delay time of 400 ps and the temperature of the sample was increased at a rate of 5 C/min. In this measurement it is assumed that any change in the TDTR output ratio at 400 ps is due to a change in the thermal conductivity since the thermal conductivity is the only strongly

temperature dependent variable in the model. The measurements did not show an appreciable change in the thermal conductivity in the measured temperature range (Figure 17) for any of the samples. As the phase transition measured by DSC is a 2nd order transition, this result is not inconsistent with the data as the transition does not have a latent heat and a small change in heat capacity is the only expected change to the diffusive heat flow model. We thought it possible that the increased mobility of the organic component of the composite might have an effect on phonon transmission and by extension affecting heat flow, however this did not appear to be the case.

2.6 Discussion

It is our belief that the low value measured is due to both the organic layers and the high density of interfaces normal to the substrate, and is dominated by heat transfer across the interfaces. Variation of the alkyl chain length, and by extension the thickness of the organic layer, did not have an appreciable effect on the thermal conductivity of the films. This is reasonably consistent with a model of thermal transport in which the thermal conductivity is dominated by the interfacial conductance. The thermal conductivity of the superlattice should increase up to the thermal conductivity of the bulk organic component as the thickness of the organic layer increases, due to a decrease in the number of interfaces per unit thickness, however, we were unable to create clays with sufficiently thick organic layers to observe the beginning of the regime where the thermal properties of the organic component begin to dominate. The combination of low interfacial conductance with the short repeat length in the nanostructure results in the characteristics of the interface dominating the bulk thermal conductivity, while the thermal properties of the individual layers become less important.

We formulated a simple series thermal resistor model to describe the heat flow normal to the film texture, using the values of 0.13 W/mK for the thermal conductivity of the organic layer and 100 W/mK for the thermal conductivity of the clay sheet (Figure 18). The value used for the thermal conductivity of the organic layer comes from that of liquid n-dodecane at STP.²⁵ We estimate the thermal conductivity of the inorganic layer to be significantly higher than the that of bulk clay since even a bulk unmodified clay has a large number of interfaces (since the thermal conductivity of the clay layers is so much greater than that of the organic layer, the actual value is not important). Using this model, the observed data can only be fit with a significant interfacial resistance. The interfacial resistance is set as a variable and the best fit to the observed data (Fig. something) is for an interfacial boundary conductance between the organic and inorganic components of the superlattice of approximately 150 MW/m²K. This value is roughly half the observed value for a spun coat PMMA/Piranha cleaned Si interface²⁷, suggesting that the value obtained is reasonable as compared to similarly coupled interfaces. As described in the previous paragraph, due to the dominance of the interfacial thermal conductance over the thermal transport properties of the layers themselves, and the relatively narrow range of organic layer thicknesses probed, we do not observe the increase in thermal conductivity up to that of the bulk organic as the organic layer thickness is increased as predicted by the thermal series resistor model.

We see a measureable increase in the thermal conductivity of the trimethyl- terminated dodecylammonium-modified clay in comparison to both larger organic groups and the primary alkylammonium modified clay. We speculate that this small increase in thermal conductivity could be due to packing differences between the different compositions, though the data set is

not extensive enough to draw any solid conclusion and the small difference in density caused by a difference in organic group packing is difficult to detect with RBS measurements.

While it was suggested earlier that study of the thermal transport properties of similarly modified smectite clays other than montmorillonite may be reasonable, it is unlikely that a non-functional change in the clay backbone would affect the thermal conductivity appreciably. Due to the apparent dominance of the thermal conductivity within modified montmorillonites by the interfacial properties and, to a lesser extent, the thermal conductivity of the organic interlayer, any change in the clay structure would have to be drastic or provide additional functionality to affect the bulk thermal conductivity.

2.7 Figures

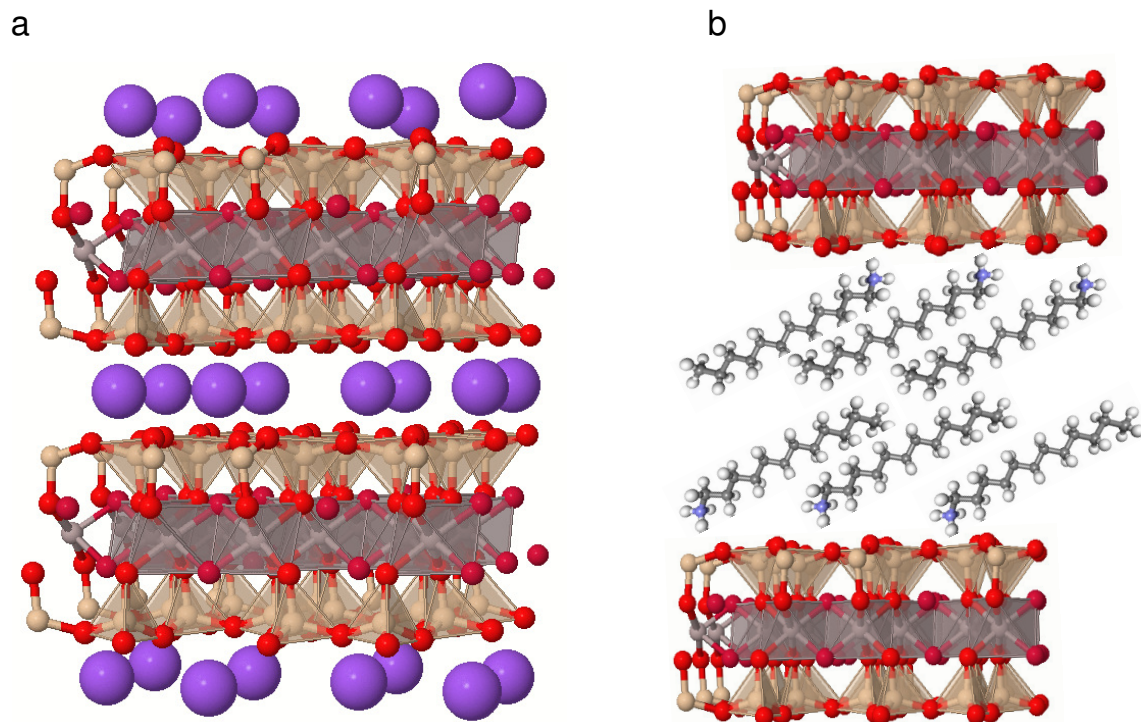


Figure 4: a. Model of the unmodified montmorillonite crystal structure. Red balls represent oxygen atoms, beige balls represent silicon or aluminum atoms and purple balls represent the charge balancing sodium atoms. b. Schematic representing an organically modified montmorillonite. This schematic does not accurately represent the interlayer packing structure.

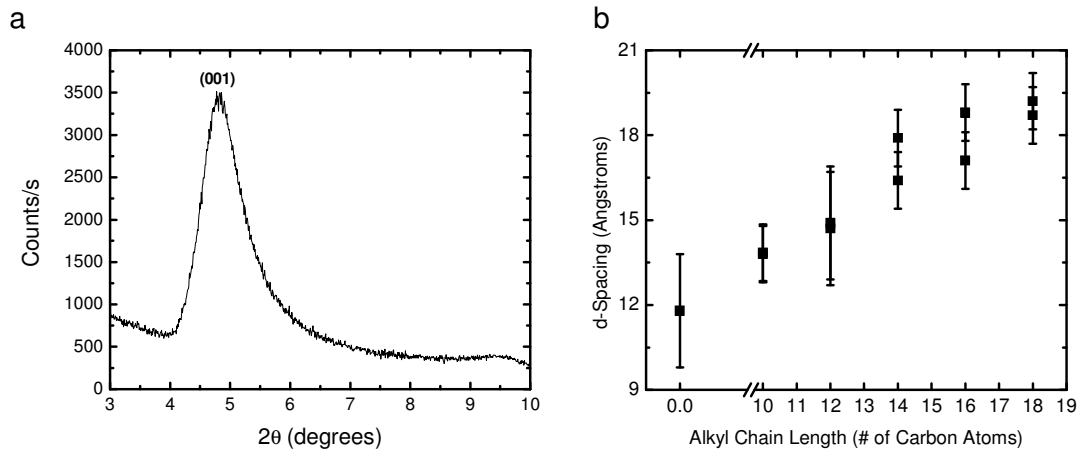


Figure 5: a. Representative θ - 2θ X-ray diffraction measurement of a dodecyl- modified montmorillonite film. b. Plot of (001) d-spacing as a function of organic functionality chain length, showing a clear increase in spacing as chain length increases. Bars refer to FWHM of the (001) peak.

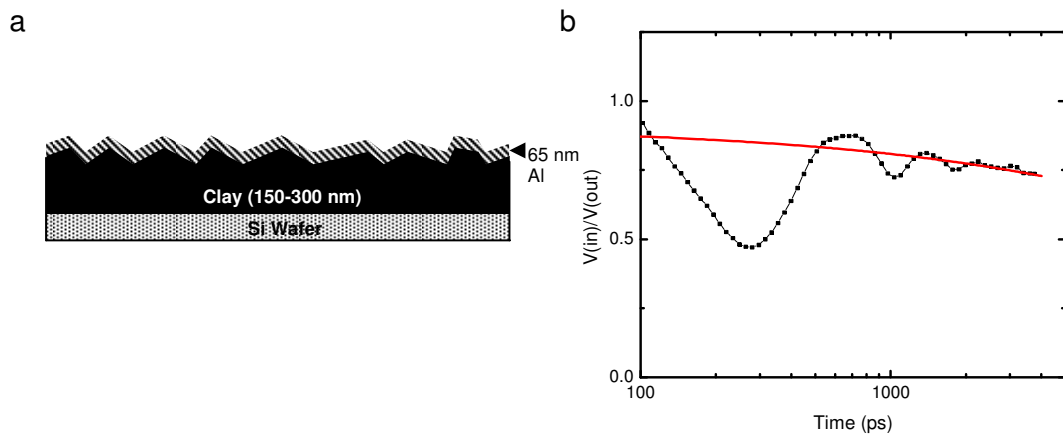


Figure 6: a. Schematic representation of the first films prepared for TDTR measurements. b. Representative TDTR data from films prepared in the geometry of the sample in Fig 4a where the long period acoustic oscillation is evident. The solid red line represents the best fit for the thermal model and shows the clay film to have a thermal conductivity of 0.13 W/mK.

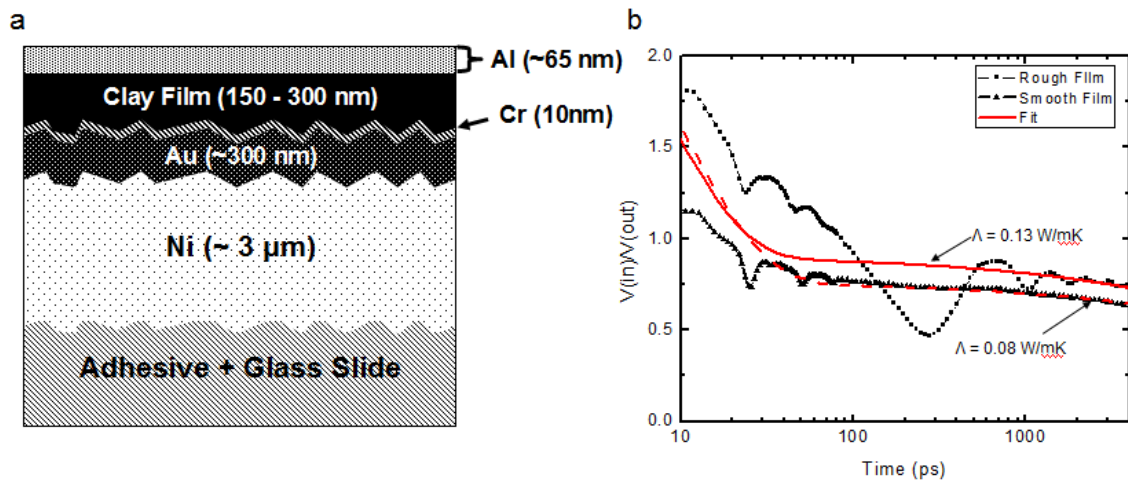


Figure 7: a. Schematic representation of the sample geometry for the smooth clay film samples. b. Comparison of TDTR data from smooth films to data from the original rough films. Both data sets are from tetradecyl- modified clay films,

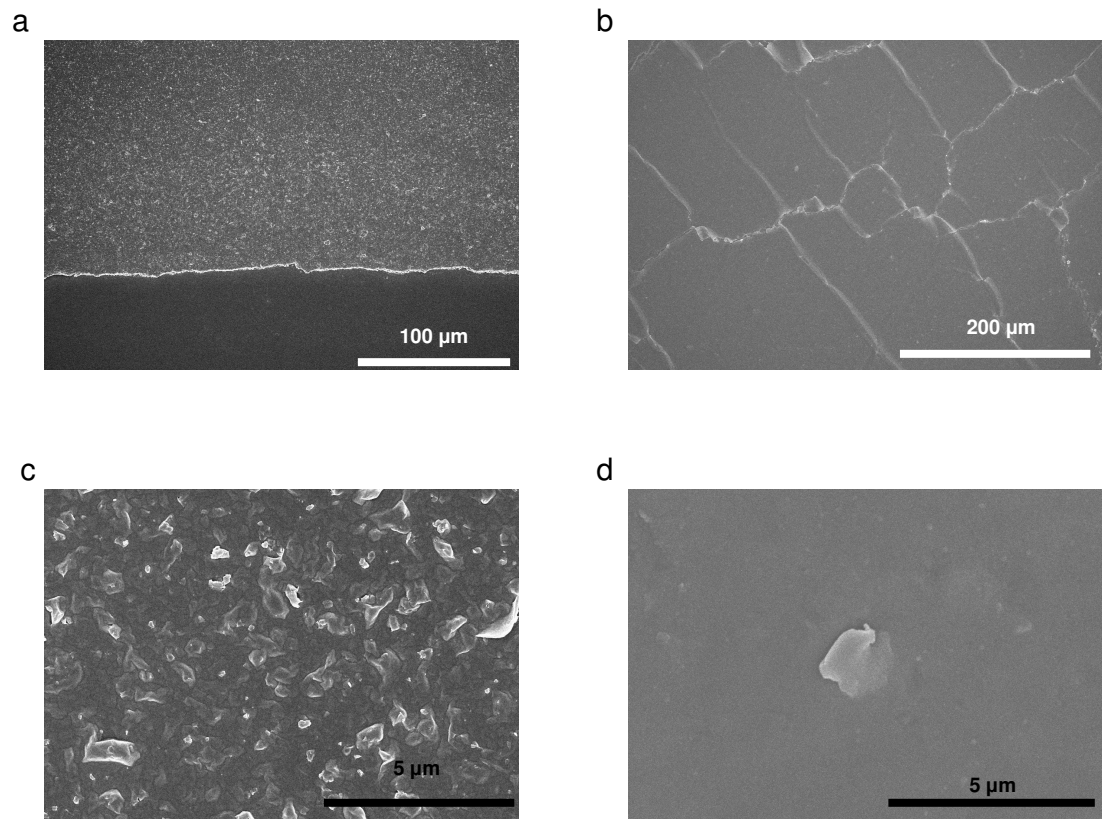


Figure 8: a and c SEM images of as-spun clay films on a Si wafer. b and d are SEM images of inverted, smooth clay films at comparable magnification to a and c.

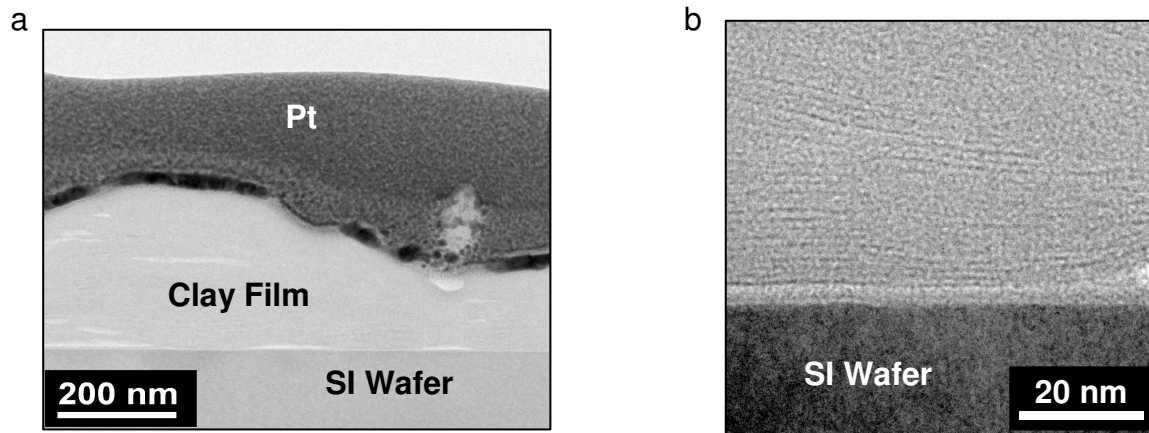


Figure 9: Cross-sectional TEM images of an organically modified clay film on a Si wafer. In b the alignment of the clay films is clearly visible to be parallel to the Si substrate.

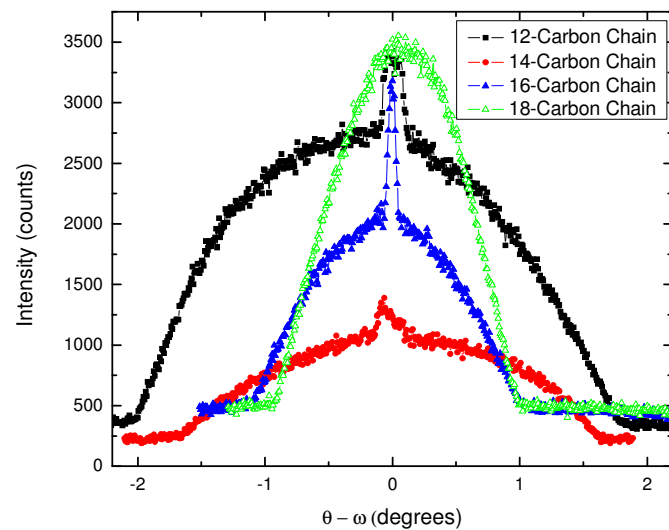


Figure 10: X-ray diffraction ω – rocking curve measurements of several organically modified clay films. In the dodecyl- to hexadecyl- modified clays, the complex distribution is evident.

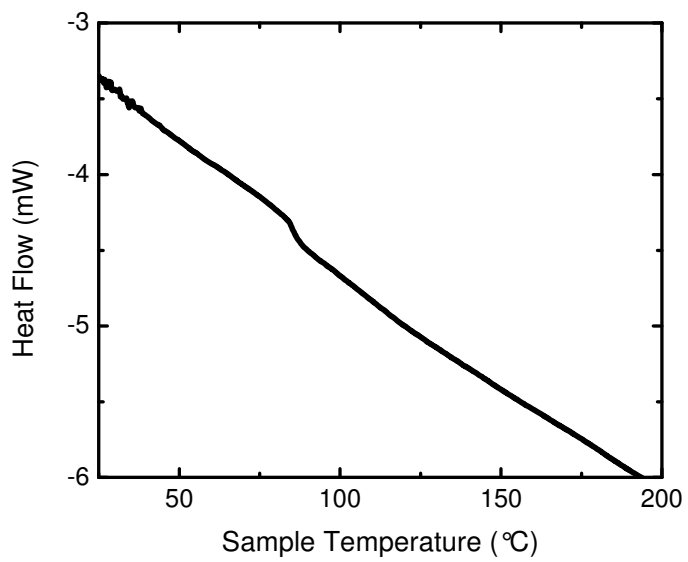


Figure 11: Representative DSC scan of dodecyl- modified montmorillonite displaying a glass-like phase transition at ~85 C. All organically modified clays display the same behavior at this temperature.

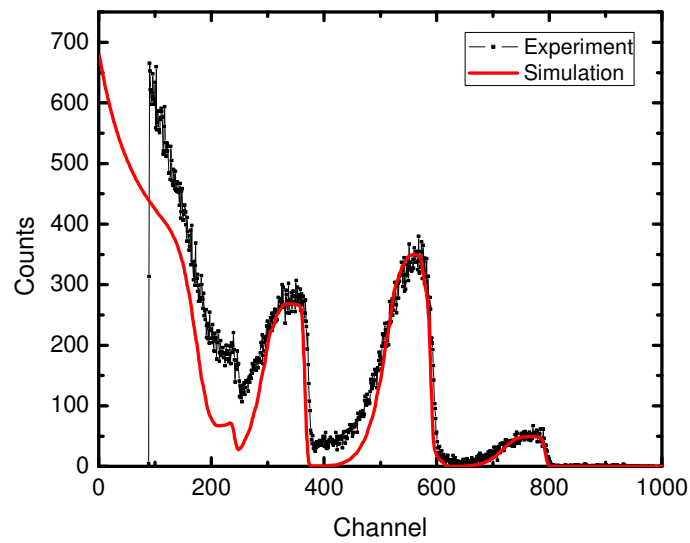


Figure 12: He^{2+} RBS measurement of a tetradecyl- modified montmorillonite film on an amorphous carbon substrate. The simulation is based on expected the expected composition of the organically modified clay film with a small Fe impurity to account for the signal from channels 700 – 800.

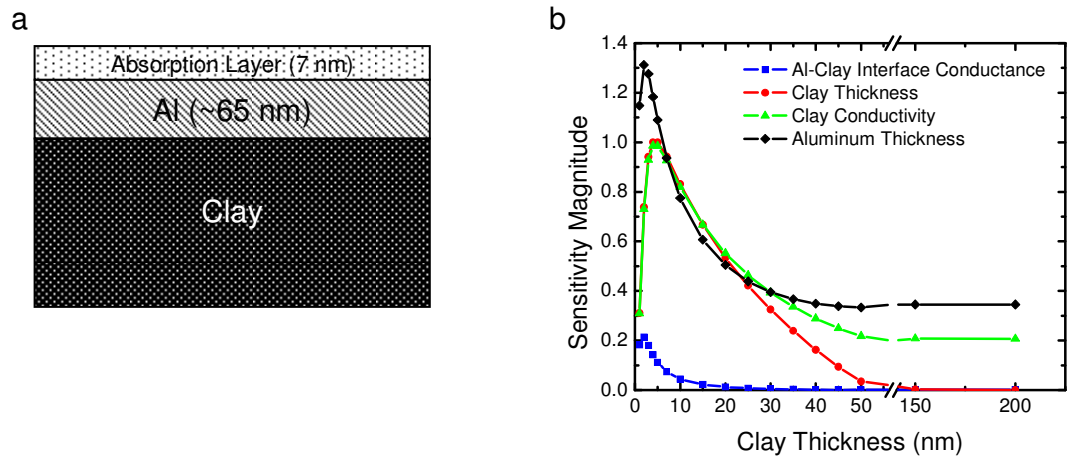


Figure 13: a. Schematic representation of the model used for the determination of the thermal conductivity. b. Sensitivity of the thermal model to several variables as a function of the clay layer thickness.

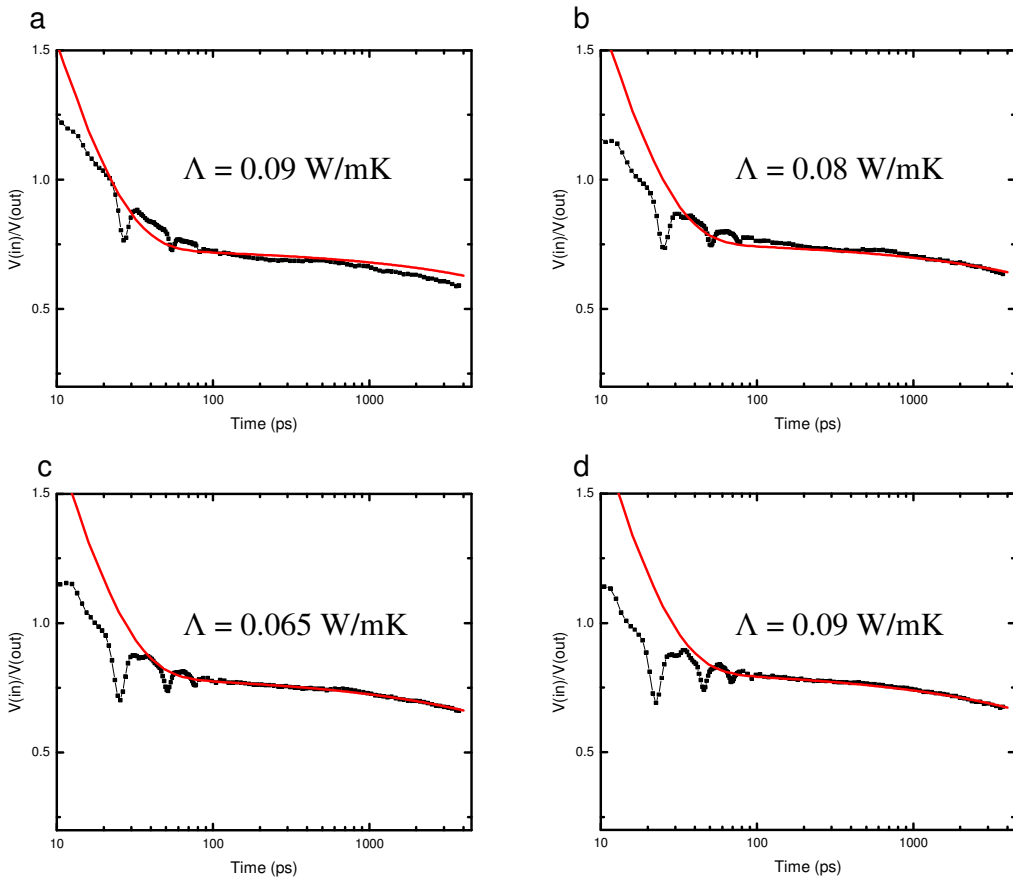


Figure 14: Parts a,b,c, and d are plots of TDTR data from dodecyl-, tetradecyl-, hexadecyl-, and octadecylammonium modified montmorillonites samples. The solid red line is the fit from the diffusive heat flow model with thermal conductivity values as reported. Data and fits here are representative of smooth organically modified montmorillonite samples.

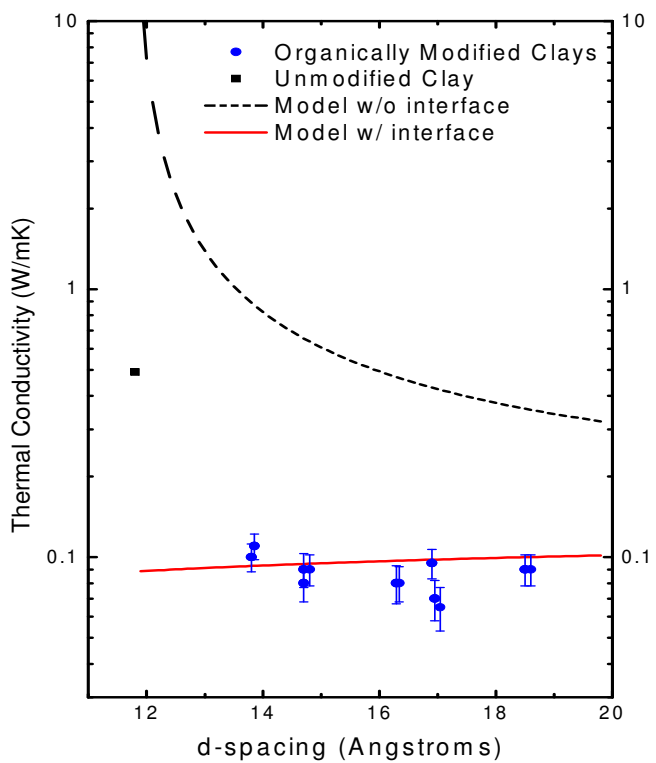


Figure 15: Thermal conductivity of montmorillonites as a function of (001) d-spacing as well as series thermal resistor models for comparison.

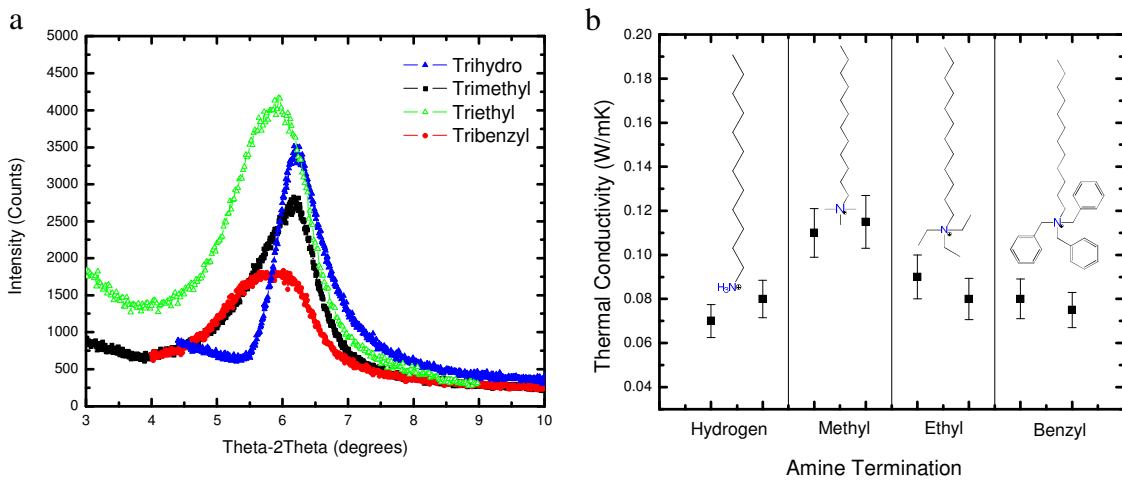


Figure 16: a. θ - 2θ X-ray diffraction measurements of tetraalkyl- modified montmorillonites showing a relative independence of the peak position on the functionalization. b. Thermal conductivity measurements of tetraalkyl- modified montmorillonite films.

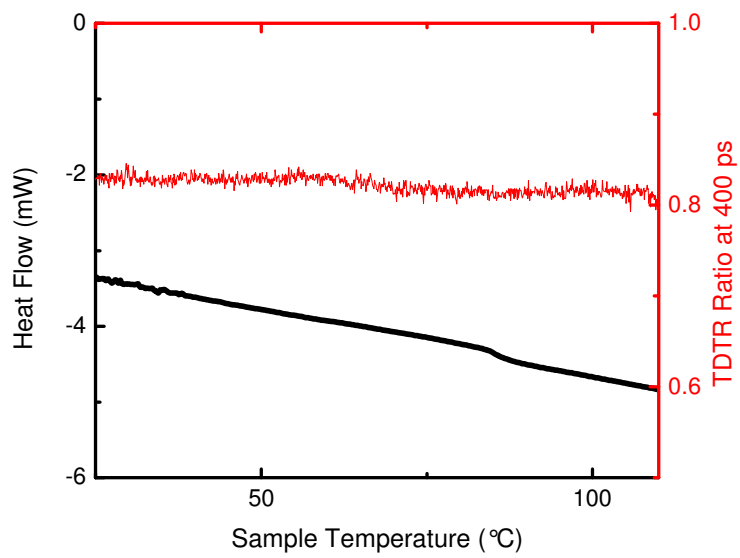


Figure 17: TDTR ratio at 400 ps of dodecylammonium modified montmorillonite film as a function of temperature plotted with a DSC trace of the same material. There was no measureable change in the thermal conductivity of the samples due to the phase transition measured in by DSC in any of the samples measured.

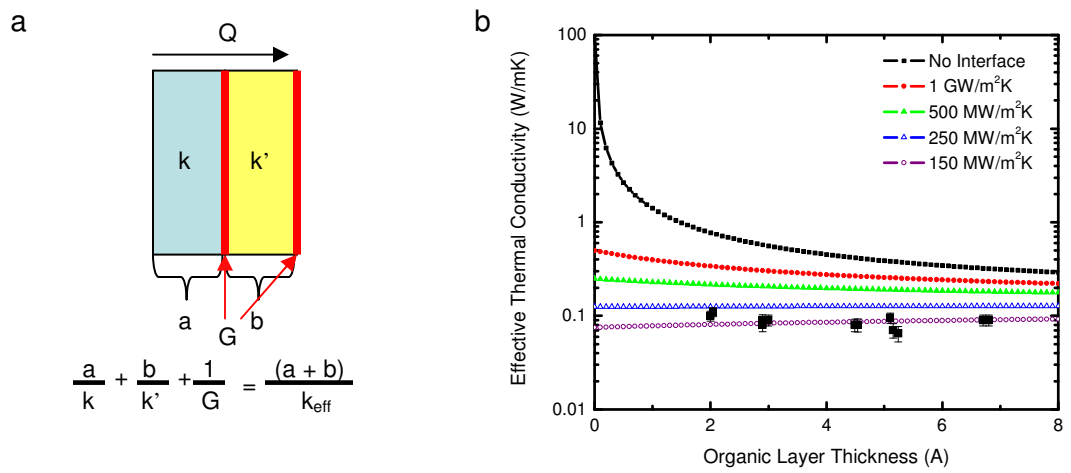


Figure 18: a. Schematic representation of the series thermal resistor model used determine the interfacial thermal conductance of the organic-inorganic interfaces of the sample. b. Plot of effective thermal conductivity as a function of organic layer thickness. Plots of the model with several values of interfacial boundary conductance are included as well as the data for the primary alkyl group modified montmorillonites.

CHAPTER 3

THERMAL TRANSPORT IN SnI_6 – ORGANIC LAYERED PEROVSKITES

3.1 Background

We have shown that the thermal conductivity of organically modified clay multilayers is strongly dependent on the interfacial thermal conductance between the clay sheets and the intercalated organic layer and the density of interfaces. Organic – inorganic perovskite structures are a nanoscopically layered system with dimensions similar to organically modified clays but with important differences.²⁸ Perovskite structures are more crystalline structures than clays as evidenced by higher order (00*l*) reflections in XRD measurements (Figure 19).²⁹ Additionally, there is flexibility in the chemistry of the perovskite backbone, providing far greater control over aspects of the inorganic component of the layered system than with organically modified clays. We chose to specifically study the thermal properties SnI_6 perovskites because of the ease of synthesis and the fact that the SnI_6 backbone is electrically conductive, providing the possibility of thermoelectric applications.

3.2 Synthesis and Characterization of SnI_6 Perovskites

SnI_6 organo-perovskites were synthesized from $\text{SnI}_2(s)$, HI (conc.) and the appropriate long chain alkylammonium group (hexyl-, decyl, and octadecyl- moieties). 1g of $\text{SnI}_2(s)$ was placed in excess concentrated HI with 2 mole equivalents of the desired alkylamine with respect to the SnI_2 . After refluxing the solution at 95 °C for 24 hours, the dark purple crystals were vacuum filtered out and were washed with a 5:1 butanol/toluene mixture. The crystals were subsequently redissolved in methanol at a concentration of 20mg/mL and the resulting solution was spin-

coated onto a silicon substrate. The resulting films were measured to be 15 - 30 nm thick by ellipsometry and appeared to be lightly purple and somewhat cloudy.²⁹

The films were shown to be highly crystalline in the (00*l*) direction by XRD measurements (Figure 18). However, SnI₆ – organic perovskites did not show the same trend toward increasing (001) spacing with increasing organic group length as the organically modified clays as evidenced in Figure 20a. XRD measurements of SnI₆ – organic perovskites show a difference in crystallinity with respect to each other inconsistent with an increase in the (001) spacing. Additionally, powder XRD measurements of various SnI₆ – organic perovskite show peaks that correspond to reflections other than the (00*l*) reflections. This indicates order in other directions which likely would increase the effective thermal conductivity due to the increase in order.

We think it likely that these differences in XRD spectra between different perovskite compositions reflect a change in the symmetry of the crystal packing as opposed to a change in spacing. While this system did not show the behavior of increasing (001) spacing with longer incorporated organic chain, this did provide the chance to investigate the effect that subtly differing crystalline symmetry has on the thermal conductivity of a layered system.

3.3 Thermal Conductivity Measurements of SnI₆ – Organic Perovskite Films

Thermal conductivities of SnI₆ – organic perovskite films were measured by the TDTR method. Measured thermal conductivities of these perovskites have did not show a dependence on the changes in crystal structure we have affected through changes of the organic group (all thermal conductivity measurements have been ~0.23 W/mK) (Figure 20d). All TDTR measurements showed a deviation from the diffusive heat flow model at long (> 800 ps) delay times, as is apparent in Figure 20c. Values for the density and thickness of the SnI₆ films for use

in the diffusive heat model was estimated from spectroscopic ellipsometry measurements and the heat capacity was estimated as a weighted average of the specific heat capacities of the components of the system. The model was unable to be modified to account for this drop in the TDTR ratio and closest fits were used accordingly.

3.4 Discussion

As of now, thermal conductivity measurements of SnI_6 – organic perovskites have shown no measureable dependence on the length of the organic group used in the synthesis. This suggests that the changes in crystal structure affected by the change in the organic component of the system do not appreciably affect the thermal transport properties. However, as the data on this system is limited, further investigation is warranted.

As for avenues of further investigation of this system, there are a few possibilities. It may be interesting to probe the effect of the strength of the organic-inorganic ionic bond by making structures with organic salts other than primary ammonium salts. This may make it possible discover the role, if any, that the organic-inorganic bond plays in heat conduction. Another possible line of inquiry could be the variation of the composition of the perovskite backbone. Through variation of the perovskite composition, it could be possible to probe the effect that the differing mass of the atoms in the perovskite has on thermal transport properties.

3.5 Figures

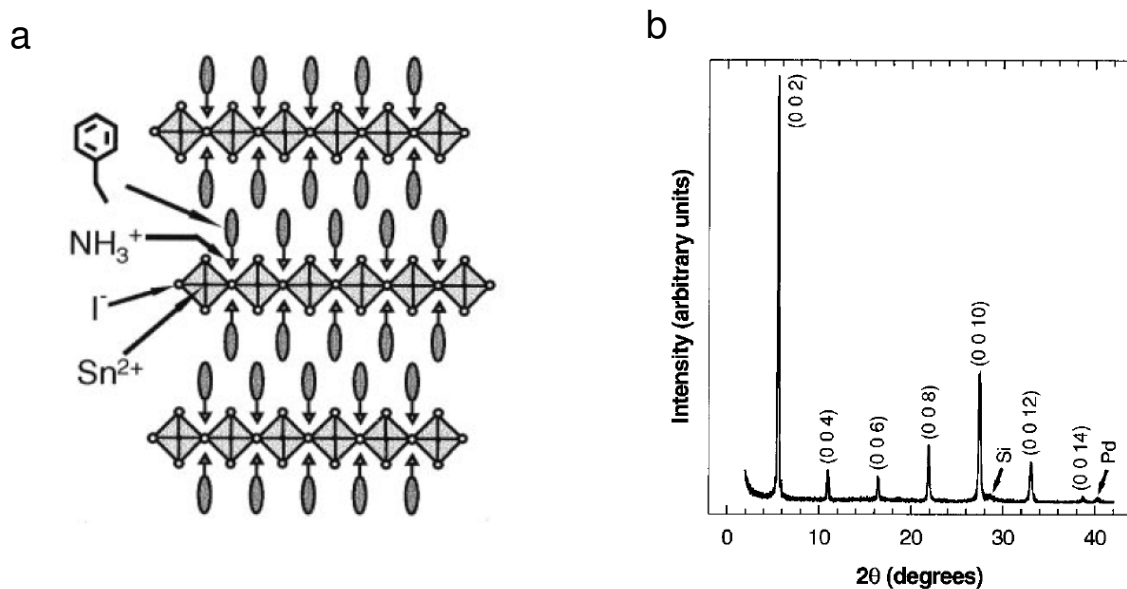


Figure 19: a. Schematic representation of SnI_6 – Organic perovskite structure. b. X-ray diffraction measurement of a SnI_6 – organic perovskite illustrating the high degree of crystallinity in the $(00l)$ direction. (Figures from Kagan *et al.*)²⁹

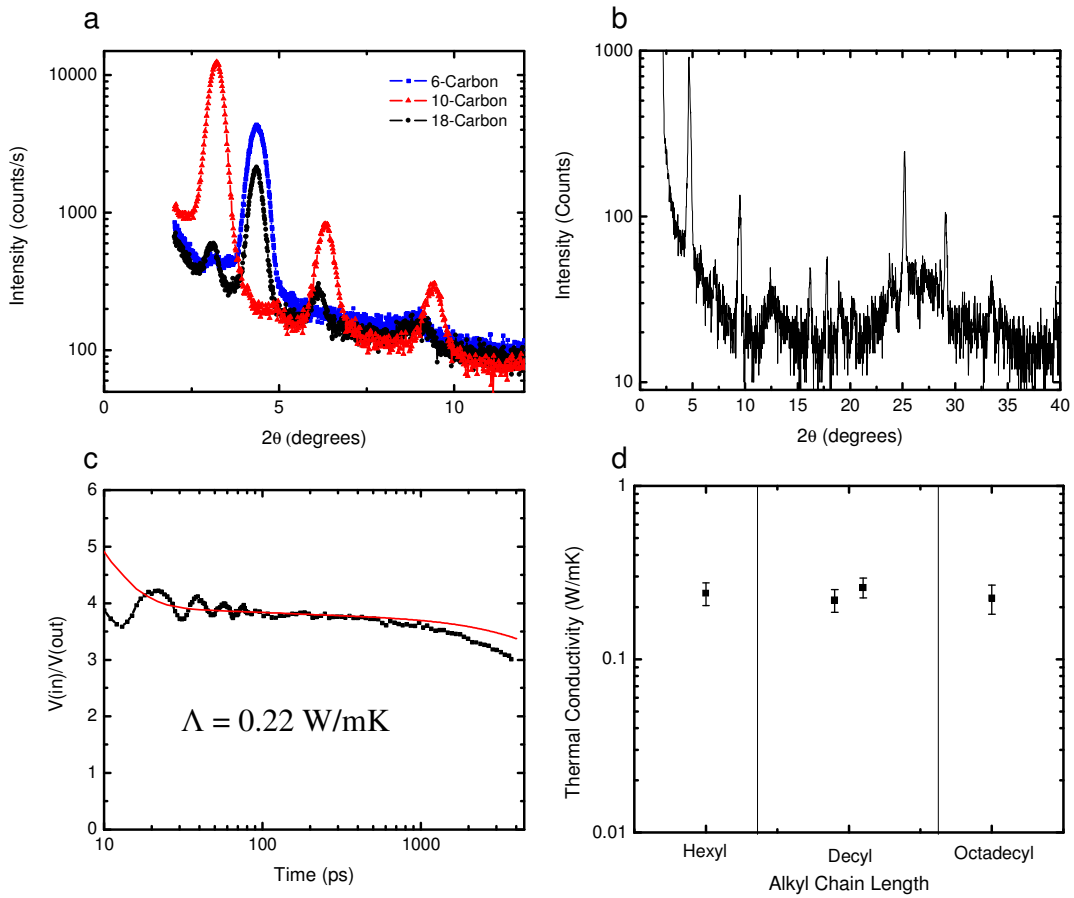


Figure 20: a. X-ray diffraction measurement of various SnI_6 – organic perovskite films illustrating a comparable level of order to results from Kagan *et al.* b. Powder XRD measurement of decylamine- SnI_6 perovksite. c. TDTR data from a 20 nm film of decylammonium- SnI_6 and the red line is the fit from the diffusive heat model with the reported thermal conductivity. d. Thermal conductivity measurements of various SnI_6 – organic perovskite films.

CHAPTER 4

CONCLUSIONS

We have investigated the effects of several variables on the thermal transport properties of organically modified montmorillonite and SnI_6 – organic perovskite films. We have determined that in the case of the organically modified clay films that thermal boundary resistance plays a dominant role in determining the bulk thermal transport properties of the film, dropping the thermal conductivity of the various alkyl-modified montmorillonites to $\sim 0.09 \text{ W/mK}$. We have also shown that it is possible to determine thermal boundary conductance values in bulk systems to a reasonable degree based on the deviation of the thermal conductivity from an idealized system. Based on the assumption that thermal transport in alkylammonium modified montmorillonites is determined in much the same way as in long-period superlattice systems, it was determined that the thermal boundary conductance between the montmorillonite sheets and the organic component of the system is $\sim 150 \text{ MW/m}^2\text{K}$. It is also surprising that a system with an almost atomic length scale repeat spacing would behave in this apparently classical manner. Additionally, data we have collected, specifically the thermal conductivity measurements of the quaternary alkylammonium modified clays, is not sufficiently explained and further investigation is needed to determine the exact cause of the anomalous thermal conductivity.

Concerning the SnI_6 – organic perovskite structures, it remains to be seen whether or not the system will show any interesting thermal transport properties. As of now, too little data has been collected to determine whether perovskites will show unusual thermal transport properties even considering the similarities between this system and the organically modified clay system, though current data shows little dependence on the crystal structure changes affected by the experiments presented here and the measured thermal conductivities measured were all

approximately 0.23 W/mK. However, the research here lays the groundwork for further inquiry into the thermal transport properties of organic-inorganic perovskite structures and provides the foundation for similar determination of boundary conductance in similarly nanoscopically layered systems.

LIST OF REFERENCES

- (1) Keesom, W. H.; Keesom, A. P. **On the heat conductivity of liquid helium-3.** *Physica* **1936**, *3*, 359.
- (2) Kaptiza, P. L. The study of heat transfer in helium-II. *J. Phys. (USSR)* **1941**, *4*, 181.
- (3) Swartz, E. T.; Pohl, R. O. Thermal Boundary Resistance. *Rev. Mod. Phys.* **1989**, *61*.
- (4) Khalatnikov, I. M. *Zh. Eksp. i Teor. Fiz.* , *22*, 687.
- (5) Swartz, E. T. Solid-solid thermal boundary resistance. *Ph.D. Thesis (Cornell University)* .
- (6) Cahill, D. G. et al. Nanoscale Thermal Transport. *J. Appl. Phys.* **2003**, *93*, 793.
- (7) Harman, T. C.; Taylor, P. J.; Walsh, M. P.; LaForge, B. E. **Quantum Dot Superlattice Thermoelectric Materials and Devices.** *Science* **2002**, *827*, 2229.
- (8) Cahill, D. G.; Watson, S. K.; Pohl, R. O. *Phys. Rev. B* **1992**, *46*, 6131-6140.
- (9) Costescu, R. M.; Cahill, D. G.; Fabreguette, F. H.; Sechrist, Z. A.; George, S. M. *Science* **2004**, *303*, 989.
- (10) Chiritescu, C. e. a. *Science* **2007**, *315*, 351-353.
- (11) Koh, Y. K.; Cao, Y.; Cahill, D. G. et al. *Advanced Functional Materials* **2009**, *19*, 610-615.
- (12) Pernot, G.; Stoffel, M.; Savic, I.; Pezzoli, P.; Chen, e. a. Precise control of thermal conductivity at the nanoscale through individual phonon-scattering barriers. *Nature Materials* **2010**, *9*, 491.
- (13) Ren, S. Y.; Dow, J. D. *Phys. Rev. B* **1982**, *25*, 3750.
- (14) Simkin, M. V.; Mahan, G. D. *Phys. Rev. Lett.* **2000**, *84*, 92.
- (15) Venkatasubramanian, R. *Phys. Rev. B* **2000**, *61*, 3091.
- (16) Chakraborty, S.; Kleint, C. A.; Heinrich, A.; Schneider, C. M.; Schumann, J.; Falke, M.; Teichert, S. *Appl. Phys. Lett* **2003**, *83*, 418.
- (17) Lee, S. M.; Venkatasubramanian, R. *Appl. Phys. Lett* **2008**, *053112*.
- (18) Touzelbaev, M. N.; Zhou, P.; Venkatasubramanian, R.; Goodson, K. E. *J. Appl. Phys.* **2001**, *90*, 763.
- (19) Cahill, D. G. *Rev. Sci. Instrum.* **2004**, *75*, 5119.
- (20) O'Hara, K. E.; Hu, X. Y.; Cahill, D. G. *J. Appl. Phys.* **2001**, *90*, 4852-4858.
- (21) Ge, Z.; Kang, Y.; Taton, T. A.; Braun, P. V.; Cahill, D. G. *Nano Letters* **2005**.
- (22) Gianellis, E. P. Polymer Layered Silicate Nanocomposites. *Advanced Materials* **1996**, *1*, 29.
- (23) Heinz, H.; Vaia, R. A.; Krishnamoorti, R.; Farmer, B. L. *Chem. Mater.* **2007**, *19*, 59.
- (24) Vaia, R. A.; Teukolsky, R. K.; Gianellis, E. P. *Chem. Mater.* **1994**, *6*, 1017.
- (25) Tanaka, Y. e. a. *International Journal of Thermophysics* **1988**, *9*.
- (26) CRC Handbook of Chemistry and Physics, 92nd Edition. Published June 15, 2011. CRC Press.
- (27) Losego, M. D. et al. *Appl. Phys. Lett.* **2010**, *97*, 011908.
- (28) Mitzi, D. B. *Prog. Inorg. Chem.* **1999**, *48*.
- (29) Kagan, C. R.; Mitzi, D. B.; Dimitrakopoulos, C. D. *Science* **1999**, *286*, 945.